21st Australasian Fluid Mechanics Conference
Adelaide, Australia
10-13 December 2018

Suitability of Different Numerical Models for Simulating Flow over a Hemispherical Protuberance

P. Enshaei[1,2], J. McCarthy[3], M. Giacobello[3], B. Thornber[2]

[1]School of Engineering
University of Glasgow, Glasgow, United Kingdom

[2]School of Aerospace, Mechanical, Mechatronic Engineering
University of Sydney, Sydney, New South Wales 2006, Australia

[3]Aerospace Division
Defence Science and Technology Group, Melbourne, Victoria 3207, Australia

Abstract

This study presents a suitability assessment of three (3) different CFD RANS models and a Delayed Detached Eddy Simulation (DDES) model, in predicting flows over a surface-mounted hemisphere. Three different diameter-based Reynolds number flows are simulated and the hemisphere surface-pressure distributions compared against new experimental data. It is found that a region of laminar flow on the windward side of the hemisphere exists, hence leading to a laminar-turbulent transition region for a thin boundary layer. The Transition SST model obtains the closest predictions to the experimental data out of the RANS models tested. Unsteady-RANS was found unsuitable for the prediction of unsteady pressure fluctuations and limitations for DDES are highlighted.

Introduction

Flows over surface-mounted hemispheres are complex and highly three-dimensional. Hemispheres are commonly found in engineering applications; from dome shaped buildings, to observation structures on submarines, to external sensor housings on aircraft. The flow-induced, unsteady pressure variations on the hemisphere may lead to undesirable structural vibrations and/or interference with nearby objects. A good understanding of flows over hemispheres is therefore important for design and operation purposes.

So far, experimental investigations have provided fundamental insights into the flow features that surround a surface-mounted hemisphere. A study by Savory and Toy [6], as part of a series of investigations, examined three different boundary layers for a range of Reynolds numbers between 1.31×10^4 to 1.4×10^5 based on the definition $Re_D = \rho UD/\mu$, where ρ is density, U is flow speed, D is hemisphere diameter and μ is dynamic viscosity. The overall drag was found to decrease with increasing Reynolds number due to a reduction in the surface pressure maxima and minima. Surface pressure measurements showed maximum and minimum pressures at $20°$ and $75-80°$ respectively on the meridian line in the symmetry plane. This result was roughly in agreement with an earlier study by Taniguchi et al. [8], who further noted the separation point at $86-88°$, independent of the Reynolds number.

Considering parametric analyses of hemisphere-induced flows, an experimental approach may become prohibitively expensive or not be possible at operational conditions. Computational Fluid Dynamics (CFD) models may provide a more cost-effective method to parametrically analyse the flow, but different models available must be validated against experimental data to ensure accurate predictions of key flow physics. Whilst there has been hemisphere-flow research carried out using various CFD models, only a few studies investigated the possibility of using robust Reynolds-Averaged Navier-Stokes (RANS) models which have been developed for engineering applications. A number of investigations regarding hemispheres in turbulent flow have made use of Large Eddy Simulations (LES) [2,9]. Most recently, an extensive experimental and numerical study by Wood et al [12] used LES to compare data for both sets of results in terms of velocity and Reynolds stress profiles. The numerical results showed good agreement with experimental results, but were obtained at high computational cost. The use of RANS models could enable rapid predictions of hemisphere induced flow fields.

The structure of the paper is as follows. The first section introduces the governing equations and method, the second presents the computational setup and grid and statistical convergence. This is followed by a presentation and discussion of the results and finally the key conclusions are summarised.

Governing Equations and Numerical Methods

The difficulty of modelling turbulence has led to the development of various approaches, each consisting of different advantages. As this study focuses on the suitability of different turbulence models for an engineering CFD application, the use of Direct Numerical Simulations (DNS) and LES were deemed unsuitable due to their high computational requirements. Therefore, the decision to use Reynolds-Averaged Navier-Stokes (RANS) models was made due to their low computational requirements in exchange for reasonable accuracy in a wide range of applications.

Using Reynolds Decomposition to separate the instantaneous velocity into a mean and fluctuating component, the continuity and Navier-Stokes equations can be given in their averaged form for incompressible flow, as shown in equation 1 and equation 2 respectively [11].

$$\frac{\partial \bar{u}_i}{\partial x_i} = 0 \tag{1}$$

$$\frac{\partial \bar{u}_i}{\partial t} + \bar{u}_j \frac{\partial}{\partial x_j}(\bar{u}_i) = -\frac{1}{\rho}\frac{\partial \bar{p}}{\partial x_i} + \frac{\partial}{\partial x_j}(\nu \frac{\partial \bar{u}_i}{\partial x_j} - \overline{u_i' u_j'}) \tag{2}$$

The three RANS models chosen throughout this investigation make use of the Boussinesq hypothesis, shown in equation 3, as a method of closing the governing equations.

$$-\overline{u_i' u_j'} = \nu_t \left(\frac{\partial u_i}{\partial x_j} + \frac{\partial u_j}{\partial x_i}\right) - \frac{2}{3} k \delta_{ij} \tag{3}$$

Based on preliminary simulations, previous literature, and the low inflow turbulent intensity, three different RANS models

were selected to assess their suitability in modelling hemisphere-induced flows:

1. Menter's $k-\omega$ SST model [3] was chosen due to its suitability for flow separation from smooth surfaces as a blend of the standard $k-\omega$ and $k-\epsilon$. This model closes the RANS equations through the addition of two extra transport equations in terms of turbulent kinetic energy, k, and specific dissipation rate, ω.
2. A laminar-turbulent transition model, the Intermittency SST (γ) [5], was assessed with the inclusion of an extra transport equation for flow intermittency, γ, in the SST formulation.
3. The second transition model assessed was the Transition SST ($\gamma - Re_\theta$) [4], which differs from the Intermittency model by a further transport equation for the momentum thickness Reynolds number, Re_θ. While solving four extra equations for the Transport SST model increases the computational power requirements, there is a dependency of Re_θ on the local flow velocity, which may lead to more accurate transition predictions.

The Transition SST model was further applied for unsteady simulations, though based on the literature review and preliminary simulations; unsteady RANS (URANS) was immediately deemed unsuitable for modelling the unsteady flow features surrounding a hemisphere, as will be seen in the results. Detached Eddy Simulation (DES) was therefore used for the unsteady simulations. DES allows the combination of URANS applied in the regions closer to the wall with an attached boundary layer, and LES in the detached regions where varying sized eddies exist [10]. To avoid grid-induced separation caused by the refined mesh in the near wall region [7], Delayed DES (DDES) was applied throughout this investigation.

The implicit pressure solver in ANSYS Fluent, utilising the SIMPLE pressure-velocity coupling scheme, was chosen based on suitability for low speed flows. A bounded central differencing scheme was applied for the convective terms in the unsteady simulations with the remaining terms discretised using a second-order upwind scheme, similarly to the steady state simulations. Second-order implicit discretisation was used for the temporal domain.

Computational Setup

Two separate computational domains were used throughout this study. The RANS models were applied using the half model shown in figure 1, alongside the given boundary conditions. To create a full model for the URANS and DDES simulations, the half model was mirrored about the symmetry plane. Apart from the symmetry condition, identical boundary conditions were used between the half and full models.

A structured mesh was generated using ANSYS ICEM, which consisted of an o-grid extending for 3-diameters (3*D*) in each direction (figure 2). The complete computational grid was given as 10*D*, 8*D*, and 4*D* in the streamwise (*X*), lateral (*Y*), and wall-normal (*Z*) directions respectively. The first cell height and growth rate were chosen to fully resolve the boundary layer on the lower wall, where the first cell z^+ value is below unity and the growth rate ranges from 1.05 to 1.15 throughout the mesh refinement study.

Three Reynolds numbers, $Re_D = 5\times10^4$, 6.4×10^4, and 1.25×10^5 were investigated. The Reynolds number for the test cases was altered through changes in the freestream velocity. The boundary-layer characteristics are shown for all test cases in Table 1. To allow validation against existing experimental and computational results, test case A is based on the flow conditions used by Wood et al [12]. The inlet conditions were prescribed as velocity and normal Reynolds stress profiles. Turbulent flow relations [1] were then used to estimate turbulent kinetic energy (k) and specific dissipation rate (ω) from the Reynolds stresses.

Test cases B and C were used to compare against experimental data provided by Defence Science and Technology (DST), conducted at the Research Wind Tunnel (RWT) facility. Here, the inlet conditions including velocity, kinetic energy and dissipation rate profiles were generated using a precursor simulation which comprised a flat plate boundary later with periodicity imposed between the inlet and outlet faces. The resultant velocity and turbulent kinetic energy profiles were then imported into the main simulation from the precursor. All test cases had relatively low freestream turbulent intensity of 0.5%. The mean streamwise velocity and k profiles for all test cases are shown in figure 3.

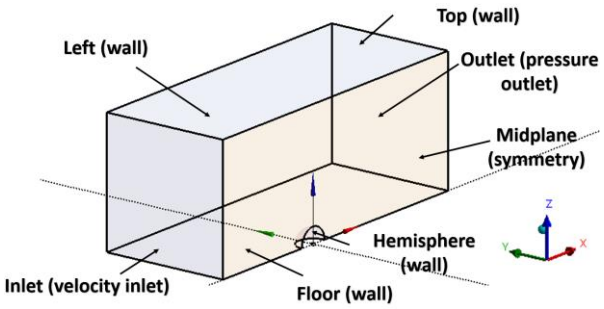

Figure 1. Computational domain and boundary conditions for the half model

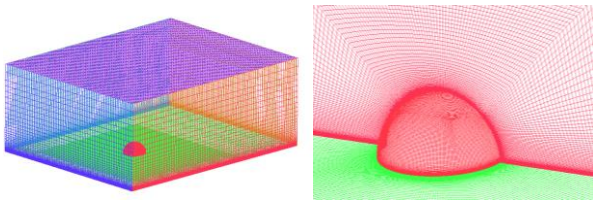

Figure 2. Meshing strategy (left: fluid domain, right: o-grid shown on the hemisphere and midplane)

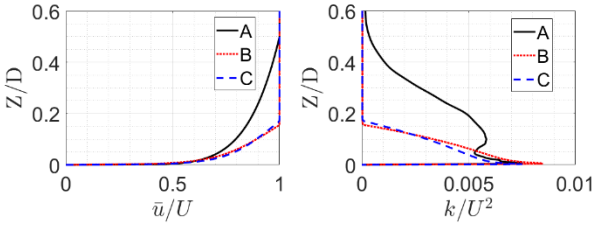

Figure 3. Inflow profiles (left: mean streamwise velocity ($\bar{u}$) right: turbulent kinetic energy (k))

Test Case	Re [$\times 10^4$]	δ/R
A	5	1.0
B	6.4	0.31
C	12.5	0.34

Table 1. Boundary layer flow characteristics for all test cases. Each test case was simulated using three RANS models, DDES and URANS, leading to a total of 15 simulations. R is the hemisphere radius, which is $D/2$, and δ is the $0.99U$ boundary-layer thickness.

To ensure grid independency for both steady and unsteady simulations, three mesh sizes based on the number of cells for each model were tested; 2, 4 and 8 million cells for steady state and 1, 2, and 4 million cells for unsteady simulations due to computational limitations. Mean surface-pressure distributions, velocity profiles and drag coefficients, in addition to velocity and surface-pressure fluctuations for unsteady simulations were monitored to ensure grid independency for each model. A similar strategy was conducted for the temporal convergence with two time-step sizes and three sampling periods tested using the same parameters. The final results were obtained using a sampling period of 1 second, allowing ten complete cycles of the longest shedding period. A sampling rate of 50 kHz was applied.

Results and Discussion

The results presented are in terms of surface-pressure distributions as a function of hemisphere's stream-wise centreline angle ϕ, shown for DDES results in figure 4. In figure 4, iso-surfaces of the Q-criterion at $Q = 5000s^{-2}$ for test case A, coloured by mean streamwise velocity, are displayed. In the upstream region, region 1, it can be seen that the two largest horseshoe vortices wrap around the hemisphere and subsequently interact with the wake flow, where hairpin vortices are present, region 3. The oncoming flow attaches to and subsequently accelerates over the hemisphere, with flow separation occurring near the hemisphere apex, region 2. The nature of the separation can be laminar or turbulent based on the boundary layer inflow conditions as further discussed below.

Mean Surface Pressure

Figure 5 presents the pressure coefficient C_p against ϕ for test case A, compared with DDES and two previous experimental datasets. While the turbulence intensities in [6] and [8] are not identical to those in test case A, the results are qualitatively, and to some extent quantitatively, in agreement. The stagnation point, identified by peak positive C_p, is located at $\phi = 20°$ for all numerical models. This agrees with previous results claiming boundary layer independency for the stagnation point [6,8]. Similarly, peak suction is well predicted by all models except for the Intermittency SST, where an earlier peak suction with lower magnitude is predicted. Interestingly, the fully turbulent $k-\omega$ SST model predicts similar results to the Transition SST and DDES models, possibly indicating turbulent separation for this test case. Numerical predictions of surface pressure on the hemisphere lee-side agree qualitatively with the experimental results, though pressure recovery is over-estimated.

The surface-pressure distributions for test cases B and C compared with experimental results from DST are shown in figures 6 and 7 respectively. A significant change in magnitude for the maximum pressure is found between test cases A and B with a relatively small change for B and C. This could suggest a stronger influence of oncoming boundary-layer thickness, compared to Reynolds number, on the location as well as magnitude of peak C_p. This supports findings by Taniguchi et al. [8] regarding the effect of boundary- layer characteristics on resultant pressure distribution.

The maximum suction for test case B occurs at a lower value of ϕ compared with test cases A and C, which likely indicates earlier, possibly laminar, separation. Furthermore, a significant increase in peak suction magnitude, and a shift downstream to $\phi \approx 80°$, is observed with increasing Reynolds number between cases B and C, indicating sub-criticality of the flow regime. As with test case A, pressure recovery was over-estimated by all models in test cases B and C.

It is worth noting the discrepancy between the numerical models and the experimental data with regards to stagnation location, for test case B. Although this is in disagreement with previous literature claiming boundary layer independency for the stagnation point, the oncoming boundary-layer thickness for test case B was significantly smaller than previous experiments. The unsteady simulations here revealed stream-wise oscillations of the main horseshoe vortex, which may cause temporal variations in stagnation- point location, though this is cause for further investigation.

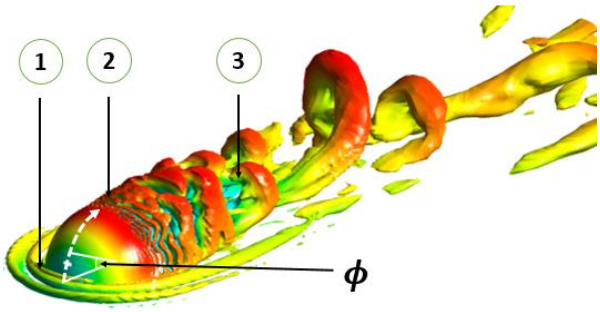

Figure 4. DDES result: Iso-surfaces of the Q-criterion for test case A, coloured by the mean streamwise velocity. The centreline angle is highlighted. Three regions of interests are labelled: 1) horseshoe vortices, 2) flow separation and 3) wake flow.

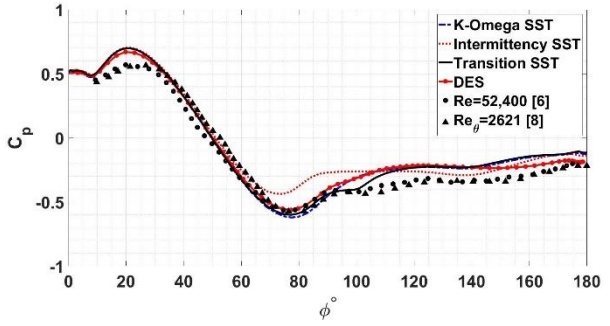

Figure 5. Mean pressure coefficient distribution over the meridian line for test case A against published experimental results.

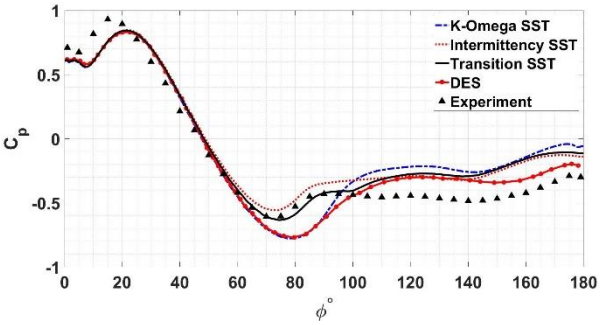

Figure 6. Mean pressure coefficient distribution over the meridian line for test case B against DST experimental results.

Although the $k-\omega$ SST model displayed encouraging results for test cases A and C, the model failed to predict the change in peak suction for test case B. Also, the Intermittency SST model under-estimated the peak suction for all three cases. The Transition SST was most successful at predicting pressure distribution up to flow separation, with demonstrated flexibility regarding boundary-layer characteristics. This could be due to the addition of the transport equation for Re_θ, compared to a combined correlation used for the Intermittency

model. Surprisingly, the DDES results are comparable to the $k-\omega$ SST model predictions. However, the DES model fails to adjust for the change in boundary-layer conditions, hence over-estimating pressure for test case B.

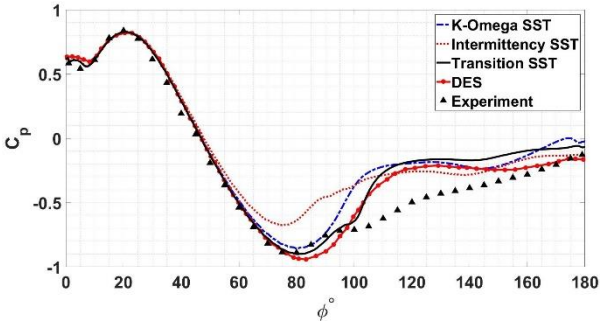

Figure 7. Mean pressure coefficient distribution over the meridian line for test case C against DST experimental results.

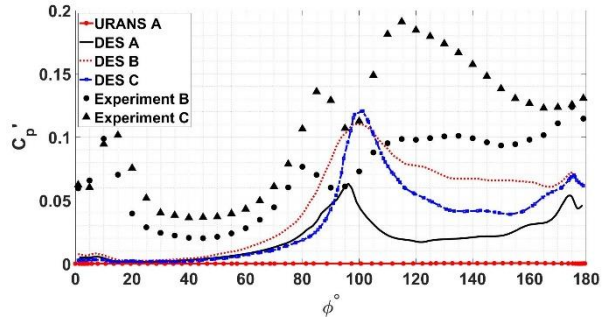

Figure 8. RMS C_p' over the hemisphere centreline for all test cases against DST experimental results. Only the results from test case A are shown for the URANS simulations.

Unsteady Surface Pressure

The root-mean-square (RMS) of unsteady pressure coefficient C_p' is plotted against ϕ in figure 8. The DDES results from all three test cases, alongside URANS for test case A and DST experimental results for test cases B and C are presented. As shown, there are no significant fluctuations noted from the URANS simulations. Therefore, only the results from the URANS simulation for test case A are included in the figure. The pressure-fluctuation magnitudes predicted by DDES are significantly lower than the experimental results. A probable cause is the activation of URANS, rather than LES, in the horseshoe vortex region as well as the lower lee-side of the hemisphere, hence leading to insignificant pressure-fluctuation predictions in these regions. Furthermore, it is known that the peaks in pressure fluctuations are likely associated with flow separation. Thus, the twin peaks in experimental results for test case C may reveal an initial laminar separation before reattachment and a turbulent separation. The DDES model only predicts one peak for test case C, and furthermore predicts delayed separation. Therefore, it may be reasonable to assume that further investigative work, using the DES model may be required to address the discrepancy in pressure fluctuations.

Conclusion

A suitability assessment of three RANS models, URANS, and DDES for the application of flow over a hemispherical protuberance, for three different Reynolds numbers, was conducted in this study. Based on comparing experimental and numerical results for mean and fluctuating surface-pressure measurements, conclusions are as follows.

A region of laminar flow was identified on the hemisphere windward side, with varying separation location based on the Reynolds number and boundary-layer thickness of the incoming flow. Between the different RANS models, the Transition SST model was found to be the most suitable, with adaptability shown for varying incoming flow characteristics.

Based on the lack of fluctuations in surface pressure measurements over the hemisphere, URANS was deemed unsuitable for the given geometry and test conditions. URANS was unable to capture any dominant mode, leading to a steady state solution, obtainable by RANS models.

DDES predicted similar results to the fully turbulent RANS model for mean pressure, with large discrepancies with experimental results for pressure fluctuations.

References

[1] ANSYS Fluent, Theory Guide Release 17.1., ANSYS Inc., 2016.

[2] Kharoua, N. & Khezzar, L., Large eddy simulation study of turbulent flows around smooth and rough domes, *Journal of Mechanical Engineering Science*, **227**(12), 2013, 2686-2700.

[3] Menter, F.R., Two-equation eddy-viscosity turbulence models for engineering applications, *AIAA Journal*, **32**(8), 1994, 1598-1605.

[4] Menter, F.R., Langry, R. & Volker, S., Transition Modelling for General Purpose CFD Codes, *Flow Turbulence Combust*, **77**(1-4), 2006, 277-303.

[5] Menter, F.R., Smirnov, P.E., Liu, T. & Avancha, R., A one-equation local correlation-based transition model, *Flow, Turbulence and Combustion*, **95**(4), 2015, 583-619.

[6] Savory, E., & Toy, N., Hemisphere and hemisphere-cylinders in turbulent boundary layers, *Journal of Wind Engineering and Industrial Aerodynamics*, **23**, 1986, 345-364.

[7] Spalart, P.R, Deck, S., Shur, M.L., Squires, K.D., Strelets, M.Kh. & Travin, A., A new version of the detached-eddy simulation, resistant to ambiguous grid densities, *Theoretical and Computational Fluid Dynamics*, **20**(3), 2006, 181-195.

[8] Taniguchi, S., Sakamoto, H., Kiya, M. & Arie, M., Time-averaged aerodynamic forces acting on a hemisphere immersed in a turbulent boundary, *Journal of Wind Engineering and Industrial Aerodynamics*, **9**(3), 1982, 257-273.

[9] Tavakol, M., Abouali, M. & Yaghoubi, M., Large eddy simulation of turbulent flow around a wall mounted hemisphere, *Applied Mathematical Modelling*, **39**(13), 2015, 3596-3618.

[10] Travin, A., Shur, M., Strelets, M. & Spalart, P.R., Detached-eddy simulation past a circular cylinder, *International Journal of Flow Turbulence and Combustion*, **63**(1-4), 2000, 293-313.

[11] Wilcox, D.C., *Turbulence Modeling for CFD*, La Canada, California: DCW Industries, 1998.

[12] Wood, J., De Nayer, G., Schmidt, S. & Breuer, M., Experimental investigation and large-eddy simulation of the turbulent flow past a smooth and rigid hemisphere, *Flow Turbulence Combust*, **97**, 2016, 79-119.